ADVANCED MATERIALS
www.advmat.de

www.MaterialsViews.com

An Ultrathin, Smooth, and Low-Loss Al-Doped Ag Film and Its Application as a Transparent Electrode in Organic Photovoltaics

*Cheng Zhang, Dewei Zhao, Deen Gu, Hyunsoo Kim, Tao Ling, Yi-Kuei Ryan Wu, and L. Jay Guo**

Thin metal films have many applications in optoelectronics and meta-materials. Among such films, silver (Ag) is widely used due to its excellent conductivity and low optical loss in the visible range. The performance of thin Ag film based devices largely depends on the surface morphology and thickness of the Ag layer.[1] It is very difficult to obtain a very thin and smooth Ag film due to 3D island formation during the film growth.[2] A rough surface morphology will impair the film conductivity and cause additional optical loss, even leading to nonconductive films when the islands cannot form percolation paths. Though increasing film thickness could alleviate the issue of film continuity, the low loss and homogeneity of the meta-materials are inevitably compromised.[1,3] To address the roughness issue, the widely employed approach to date is to use a 1–2 nm germanium (Ge) layer before Ag deposition,[4] which leads to a more than one order of magnitude reduction in surface roughness for thin (10–20 nm) Ag films. However, Ge is highly lossy in the visible range and therefore the transmittance of this bilayer film is reduced.

When considering the important application as transparent electrodes, thin Ag films should be semitransparent and have good conductivity. However, the 3D island growth mode not only limits the film conductivity but also causes light loss due to excitation of plasmon resonances. The most commonly used transparent conductor, indium tin oxide (ITO), suffers from poor mechanical flexibility and insufficient conductance for large-area devices, as well as rising cost due to limited indium supplies on the planet and the increasing demand for indium in displays and the related electronics market.[5] To meet this challenge, many potentially alternative transparent electrodes have been developed,[6] including graphene,[7] carbon nanotubes,[8] highly conductive polymers,[9] patterned metal grids,[10,11] metal nanostructures, and nanowires.[12–15] Carbon-based materials improve the mechanical flexibility of the electrode; however, their low conductivity largely limits electronic performance.[6] Transparent metal mesh structures[11,16–19] and metal nanowire networks[13] either require patterning or complex synthetic procedures. Moreover, both platforms only provide global conductivity; they are totally nonconductive between the wires, and therefore cannot be used directly as transparent electrodes unless an additional conducting layer is added.[16,17] Many practical applications, including large-area flexible organic photovoltaics (OPVs), still call for easily fabricated high-performance transparent conductors. A thin and continuous metal film that uses a simple deposition method is an ideal solution, and can be integrated into semitransparent smart windows[20] and tandem structures,[21,22] but so far its transmittance has been limited due to the thickness required to achieve the desired conductivity.

Here, we report an ultrathin and smooth Ag film, which shows low optical loss and low electrical resistance. This film can be made easily without applications of seeding layers and critical fabrication conditions, only involving co-deposition of small amounts of Al during Ag deposition (**Figure 1**a). The incorporation of a small amount of Al suppresses the 3D island growth of Ag and facilitates ultrathin film formation. We investigated Al-doped Ag films as transparent conductors. OPVs fabricated on such thin film electrode show enhanced power conversion efficiencies (PCEs) due to light trapping inside the photoactive layer. Moreover, our devices exhibit significantly improved bending capability and stability compared to ITO-based ones. Our findings provide a novel approach to achieve, without a wetting layer, an ultrathin and smooth Ag film with low loss and good conductivity.

Ag is known to follow the Volmer–Weber growth mode,[23] in which the deposited Ag atoms initially form isolated islands. As the deposition continues, these islands grow and eventually connect to form a semicontinuous/conductive film. The critical thickness leading to a conductive film is defined as the percolation threshold, which is typically between 10–20 nm.[24] However, the film roughness is large, with a root-mean-square (RMS) roughness value of 6 nm for a 15-nm-thick Ag film.[4]

Remarkably, by introducing a small amount of Al into Ag via a simple co-sputtering process (Figure 1a), the percolation threshold can be reduced to 6 nm. Except for the early onset of continuous film formation, the Al-doped Ag film has a smooth surface morphology with a significantly reduced RMS roughness of less than 1 nm. The scanning electron microscopy (SEM) characterization shows drastically different film morphology between the 9-nm pure Ag film (Figure 1c) and 9-nm doped Ag film (Figure 1d). The source power of the Ag target

C. Zhang,[+] Dr. D. Zhao,[+] Dr. D. Gu, H. Kim, Dr. T. Ling, Dr. Y.-K. R. Wu, Prof. L. J. Guo
Department of Electrical Engineering and Computer Science
University of Michigan
Ann Arbor, Michigan 48109, USA
E-mail: guo@umich.edu

Dr. D. Gu
School of Optoelectronic Information
University of Electronic Science and Technology of China
Chengdu, Sichuan 610054, P. R. China
[+]These authors contributed equally to this work.

DOI: 10.1002/adma.201306091

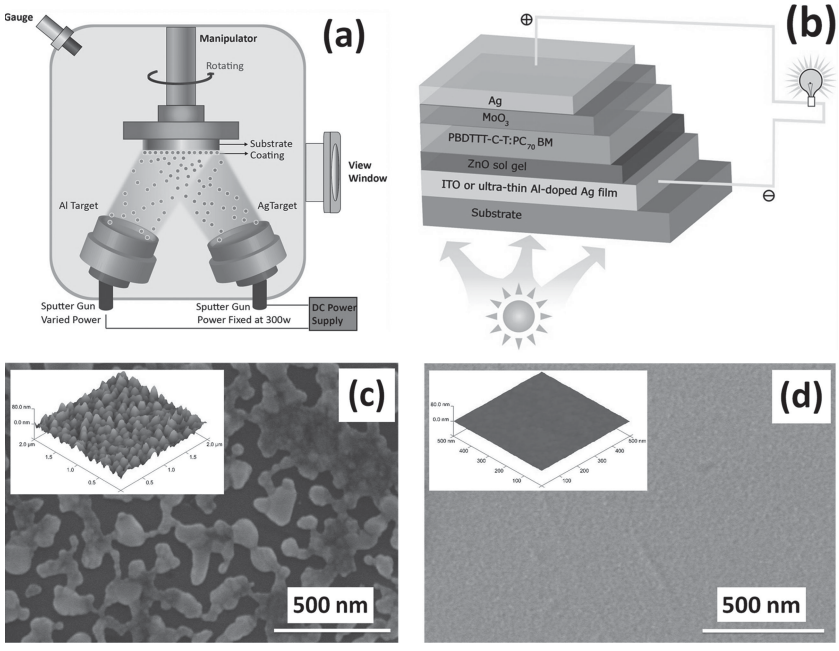

Figure 1. a) Set-up of co-deposition of Ag and Al. b) Schematic of the OPV devices with ITO or ultrathin Al-doped Ag film as electrodes. SEM images of c) 9-nm pure Ag film, d) 9-nm Al-doped Ag film. The insets in (c) and (d) are the corresponding AFM images. All films were deposited on fused silica substrates. The 9-nm pure Ag film has an RMS roughness of 10.8 nm, 12 times higher than that of the 9-nm Al-doped Ag film (0.86 nm). (For colour version see SI Fig. S12)

was held at 300 W and that of Al was 200 W, which translates into deposition rates of 0.9 and 0.06 nm s^{-1}, respectively. The grain or island like morphology in Figure 1c is typical of a pure thin Ag film. The islands are connected in some local regions, but lack long-range connections. As a consequence, the 9-nm pure Ag film is nonconductive. The localized surface plasmon resonance excitation of these islands leads to extra optical scattering loss,[25] and its corresponding transmittance spectrum is shown in Figure S1a in the Supporting Information. In sharp contrast, the 9-nm Al-doped Ag film is very uniform and smooth.

The insets in Figure 1c and 1d show the AFM images of 9-nm pure Ag and Al-doped Ag films, respectively. The RMS roughness of 9-nm pure Ag film is 10.8 nm. However, the roughness of Al-doped Ag films is over one order of magnitude lower, with an RMS value of 0.86 nm. For the Al-doped Ag films, the one with 6-nm thickness has a slightly higher roughness (0.82 nm) than that with 7-nm thickness (0.78 nm). This result is anticipated, since 6 nm is the percolation threshold for the formation of a thin, continuous film. The initial stage of the film could be more defective in its morphology than a thicker one, which would lead to its slightly higher roughness. Meanwhile, this higher roughness introduces additional optical loss, which was verified by the ellipsometry measurement as shown in the inset of **Figure 2**a. Beyond the percolation threshold at 6 nm, the roughness of the Al-doped Ag film decreases slightly when approaching 7 nm. Afterwards, the roughness increases gradually as film thickness increases. Detailed AFM images of Al-doped Ag films with different thicknesses are shown in Figure S2, with RMS roughness of less than 1 nm. The AFM image of the fused silica substrate is shown in Figure S3. Moreover, the smooth surface morphology of the Al-doped Ag film also pertains to large film thickness. As shown in the insets of Figure S4a and b, for a 100-nm thick film, the Al-doped Ag film has a lower roughness than the pure Ag film (1.1 vs. 3.6 nm). This result is also demonstrated by the SEM images taken at a 20° tilted angle shown in Figure 1c and 1d, which show different morphologies.

The Al incorporation into the Al-doped Ag film is about 10 % atomic concentration in films deposited under a combination of "300 W Ag and 200 W Al" power, as evidenced by X-ray photoelectron spectroscopy (XPS) measurements (Figure S5). Al and Ag have almost identical atomic radii (1.44 Å for Ag and 1.43 Å for Al) and the same crystalline structure (face-centered cubic). Therefore, adding a small percentage of Al into Ag film does not significantly affect the electrical and optical properties of the film. The film properties should be similar to those of pure Ag film, but with the advantages of being ultrathin and ultrasmooth.

We would like to highlight the use of the spectroscopic ellipsometry measurement as a reliable technique to accurately determine the thickness of ultrathin films and their corresponding optical properties. In general ellipsometry measurements, there is a correlation between thickness and optical constants in thin absorbing films, as the reflection/absorption depends on both the film's thickness and its optical coefficients. To break this correlation and precisely determine the film thickness/optical constants, the "interference enhancement" method was implemented by depositing the metal film on the silicon substrate with a 300-nm thermal oxide layer on top.[26] The measurement procedure is elaborated in Figure S6a. The ellipsometry data confirm the 6-nm film thickness, which is consistent with the nominal thickness based on the calibration of deposition rates. The imaginary part of permittivity is a parameter that signifies the optical loss of the film, and its values with varying film thickness are shown in the inset of Figure 2a. A huge drop of the imaginary permittivity occurs for Al-doped Ag film thickness from 6 to 7 nm, which corroborates the film roughness change described earlier. These results verify that 6 nm is the percolation threshold for Al-doped Ag film deposition, with further evidence presented later from electrical measurement.

Figure 2a shows the transmittance spectra of Al-doped Ag films with different thicknesses. All of these films are highly transparent, with an 80% transmission at 550 nm (7-nm Al-doped Ag). A small transmittance shoulder is located at around 320 nm, close to the Ag bulk plasma frequency; it is an intrinsic property that a thin Ag film becomes slightly transparent around its plasma frequency.[27] Towards the UV end, the inter-band absorption becomes significant and the transmittance drops abruptly.[28] At longer wavelengths, similar to other metals, the film behavior approaches that of a perfect

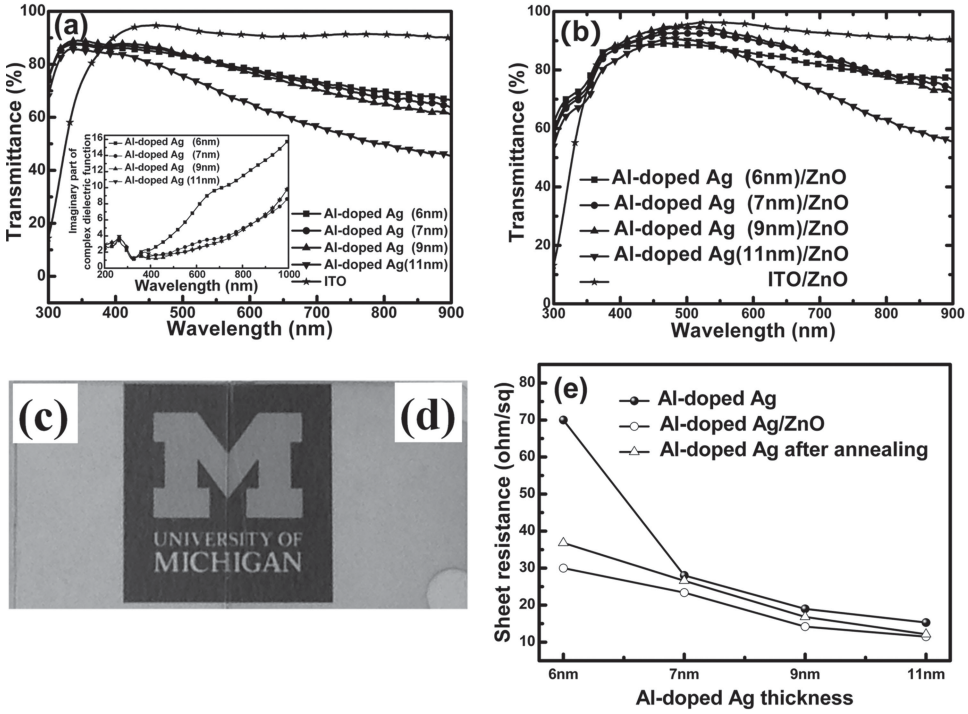

Figure 2. Transmittance spectra of a) Al-doped Ag films and b) Al-doped Ag/ZnO films with different thickness; ITO and ITO/ZnO films are also shown. Photos of c) ITO/ZnO and d) 7-nm Al-doped Ag/ZnO transparent conductors in front of a colored logo. The inset in (a) compares the dependence of the imaginary part of the complex dielectric function on the wavelength for Al-doped Ag films with different thicknesses. e) Sheet resistance vs. Al-doped Ag film thickness. (For colour version see SI Fig. S13)

conductor and its reflection increases towards the infrared regime (Figure S1b). As a consequence, film transmittance gradually drops, but still maintains a relatively high value (e.g. 65% at 900 nm for 7-nm Al-doped Ag). As a comparison, the transmittance of 9-nm pure Ag film, plotted in Figure S1a, is significantly lower than that of 9-nm Al-doped Ag film (55% versus 80% at 550 nm). There is a broad dip at around 450 nm, which results from the absorption of the cracks and voids constituting the film. Unlike a thicker Ag metal film described by the Drude model, the transmittance does not drop with the increase of the wavelength, which is caused by the separate islands within the discontinuous film. The transmittance of the Al-doped Ag film varies with thickness as well, and is relatively high even at the percolation threshold of 6 nm. As film thickness increases, the transmittance drops, which is consistent with Beer's absorption law. The transmission spectra of 7-nm films (and films with ZnO coatings) with different Al-doping concentrations were studied, as shown in Figure S7. The Ag target power was fixed at 300 W, while the Al target power was adjusted to 100, 150, 200, 300, and 400 W. The calibrated Al deposition rates at 200 and 400 W were 0.06 and 0.15 nm s^{-1}, respectively. The Al-doping concentrations were ordered from lowest to highest, with sample films denoted as L2, L1, N, H1, and H2, respectively, in which N refers to the film deposited under the optimal power condition that corresponds to ca. 10% Al atomic concentration. The L2 film has a lower transmittance than the other four, which is expected since its Al doping is the lowest, which makes the film closer to a lossy Ag film. Even such a small amount of Al promotes continuous Ag film formation. L1, N, H1, and H2 films have similar transmittance, with N and H1 films having slightly higher values than the L1 and H2 films.

The effect of Al-doping concentration on the properties of Ag films is two-sided. On one hand, doping Al greatly reduces roughness of the Ag film and promotes continuous film formation, improving its optical transmittance and electrical conductivity. Insufficient doping would not fully promote continuous film formation, as indicated in the case of L2. On the other hand, excess Al doping could introduce defects in the film, which would lead to optical loss.[29] These defects can also act as scattering sites for the free electrons in the film. Therefore, excess Al doping is detrimental (e.g., H2). The "0.9 and 0.06 nm s^{-1} rate" combination exhibits an optimal performance.

The ultrathin and ultrasmooth Al-doped Ag film introduced here satisfies the requirements of a desirable transparent electrode by its simple fabrication process, nearly flat transmission spectrum, easy device integration, and robustness. Surface roughness of electrodes is detrimental to the reliability of organic optoelectronic devices, and can originate from irregularities of the electrode itself or tiny particles adsorbed on top of its surface.[30] Since the whole device's thickness is only on the order of 100 nm, a rough surface could easily result in electrical shorts between its electrodes, especially for large-area devices. Devices with rough electrodes are prone to exhibit low efficiency due to the current shunt paths which produce higher dark current.[14] This fabricated smooth Al-doped Ag film is of significance in providing a simple solution to overcome this problem.

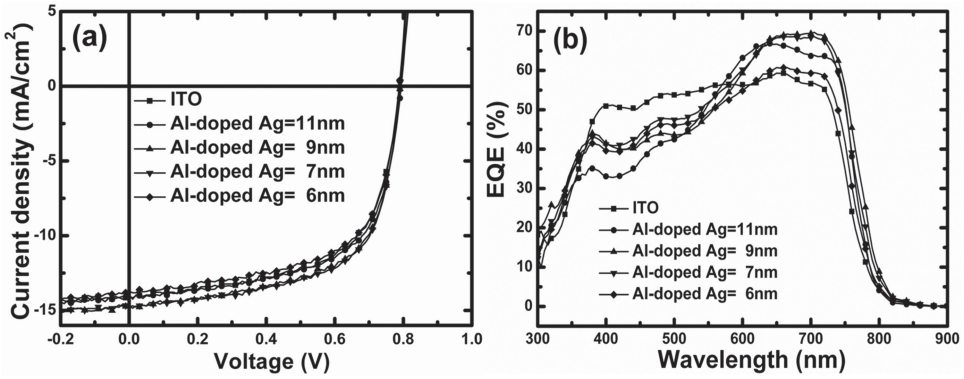

Figure 3. a) *J–V* characteristics of ITO-based and ultrathin Al-doped Ag based OPVs. b) EQEs of ITO-based and ultrathin Al-doped Ag based OPVs. (For colour version see SI Fig. S14)

This described ultrathin Al-doped Ag film has high transparency while retaining good electrical conductivity. Our film's transmittance is greater than 80 % until approximately 500 nm and drops at longer wavelengths. The increased reflection from the thin film, together with the top Ag anode as shown in the OPV device structure in Figure 1b, can be advantageously utilized to form a Fabry–Perot optical cavity to improve the optical absorption of the thin organic active layer. This strategy can increase the PCE of the OPV, especially when considering the higher photon flux of the solar spectrum in the longer wavelength region (600–800 nm).[31] In the inverted OPV structure shown in Figure 1b, 45-nm ZnO is spin-coated onto the Al-doped Ag film to work as an electron-transporting and hole-blocking layer. The overall transmittance of this structure is further increased to above 80% from 400–800 nm in the case of a 7-nm-thick electrode, exhibiting a transmittance of 92% at 550 nm as shown in Figure 2b. This result can be explained with the fact that the ZnO layer works as an anti-reflection layer (Figure S1b). The properties of these deposited films were compared to other reported works in terms of transmittance at 550 nm versus sheet resistance (Figure S8), with the ZnO-coated Al doped Ag film showing similar or superior performance. Since the ZnO thickness needs to meet other requirements for device operation, no further optimization of ZnO was carried out at this stage.

The sheet resistances of Al-doped Ag (Al-doped Ag/ZnO) films with different Ag layer thicknesses of 6, 7, 9, and 11 nm are 70 (30), 28 (23.4), 19 (14.2), and 15.3 (11.5) Ω sq^{-1}, respectively (Figure 2e). The Ag film conductivity improves as its thickness increases.[32] There is a significant drop in the sheet resistance from 6 to 7 nm film, which further supports findings that 6 nm is a percolation threshold. The conductivity of the film is further improved after ZnO coating, which is partially attributed to the baking treatment for converting ZnO sol-gel into ZnO crystalline film . To prove this, post-annealing treatment of Al-doped Ag films in a nitrogen environment was done at 150 °C for 15 min (the same temperature and time as that for baking ZnO), resulting in an observed drop in sheet resistance as shown in Figure 2e. Meanwhile, SEM images of the 9-nm Al-doped Ag film before and after the annealing treatment were taken, as shown in Figure S9, and exhibit no discernible change in morphology. These results imply that high-temperature annealing makes the doped film more conductive, and that this film is robust against high-temperature treatment. Generally, the defects and scattering sites in the thin films that affect the free electron motion can be reduced by annealing,[33] which explains the improved conductivity of the film. The sheet resistances of Al-doped Ag (Al-doped Ag/ZnO) films with different Al concentrations of L2, L1, N, H1, and H2 were also measured, and are 28.3 (22.3), 27 (21.6), 28 (23.4), 28.5 (23.9), and 29.2 (24.1) Ω sq-1, respectively (Table S1).

Al-doped Ag films were deposited with different thickness to evaluate their feasibility for use as the transparent electrode in OPVs, and their performance was compared to OPVs made with ITO electrodes. Other device layers were kept identical. The device geometry used is shown in Figure 1b. Poly[4,8-bis-(2-ethylhexyloxy)-benzo[1,2b:4,5b0]dithiophene-2,6-diyl-alt-4-(2-ethylhexyloxy)-thieno-[3,4b]thiophene-2,6-diyl] (PBDTTT-C-T):[6,6]-phenyl C71-butyricacid methyl ester ($PC_{70}BM$) forms the bulk heterojunction for the light absorption and photocurrent generation, exhibiting broad and strong absorption from 350–750 nm as shown in Figure 4b. This doped Ag film does not require any surface treatment for making the OPV device.[34] **Figure 3**a shows the comparison of the *J–V* characteristics of the devices of which the electrode is either ITO or Al-doped Ag films of different thicknesses. The main photovoltaic parameters of the devices are summarized in Table S2. An ITO-based device has a PCE of 6.87%, however, devices built on different thick Al-doped Ag films as transparent cathodes produce consistently better efficiency (a maximum PCE of 7.44% is reached at 7-nm Al-doped Ag based device). Detailed discussion can be found in the Supporting Information. Their corresponding EQE spectra also exhibit variance as shown in Figure 3b.

To understand the origin of the device efficiency enhancement, the external quantum efficiencies (EQE) and total absorption efficiency (TAE = 1 – *R*, where *R* is the measured reflection from the device[31] are plotted in **Figure 4**a, as well as relative TAE and EQE enhancement (ratio of value for 7-nm doped-Ag based device over that of the ITO-based device) in Figure 4b. The 7-nm Al-doped Ag based device shows a reduced EQE in the range from 370–580 nm. However, the EQE enhancement from 580–870 nm is evident, contributing to a large increase in the photocurrent. Quantitatively, the reduction in short-circuit

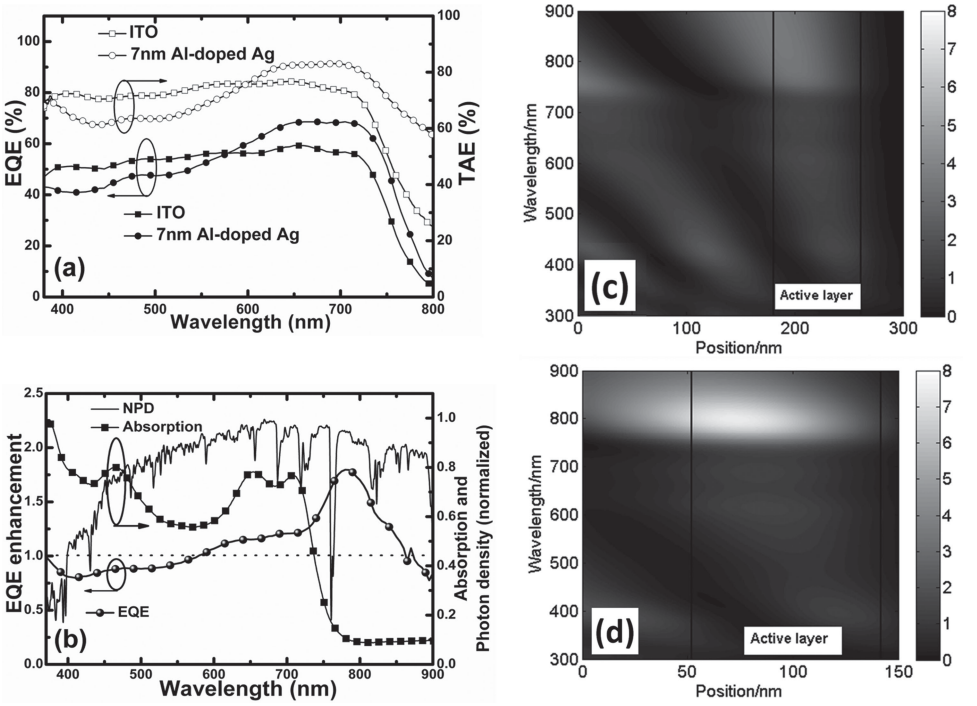

Figure 4. a) TAEs and EQEs of ITO and 7-nm Al-doped Ag based devices. b) EQE and TAE enhancements of 7-nm Al-doped Ag based device over ITO-based device, as well as the normalized absorption spectrum of PBDTTT-C-T:$PC_{70}BM$ active layer and normalized photon density of AM1.5G solar light. Simulation of the optical field intensity ($|E|^2$) distribution versus position and wavelength in c) ITO-based device and d) 7-nm Al-doped Ag based device, where the enhanced optical field in the active layer around 800 nm is responsible for the measured EQE enhancement at the same wavelength range shown in Figure 4b. (For colour version see SI Fig. S15)

current density (J_{sc}) is estimated to be 0.6 mA cm^{-2}. Meanwhile, the enhancement is estimated to be 1.4 mA cm^{-2}, which produces a total enhanced J_{sc} of 0.8 mA cm^{-2}. To further investigate the origin of the EQE enhancement in the Al-doped Ag based devices, simulations of the optical field intensity ($|E|^2$) distribution versus position and wavelength were performed for ITO and 7-nm Al-doped Ag based devices (shown in Figure 4c and 4d). This simulation is based on the 1D transfer matrix method.[35] For the 7-nm Al-doped Ag based device, a resonance cavity is formed in the active layer between the reflective top Ag anode and the semitransparent Al-doped Ag cathode, which exhibits a spectrum peak that is close to the absorption edge of PBDTTT-C-T:$PC_{70}BM$, beyond 750 nm (in the range from 750–850 nm). Such a cavity effect and the resultant increase in the optical field intensity will lead to more efficient light harvesting as the active material layer itself has low absorption in this region. Finally, the film mechanical stability on PET substrate was evaluated, where Al-doped Ag film shows excellent mechanical bendability compared with ITO (Figure S10). Meanwhile, the Al-doped Ag based device has long-term stability, as shown in Figure S11.

In conclusion, an ultrathin, smooth, and low-loss Al-doped Ag film without any wetting layer has been demonstrated by co-sputtering a small amount of Al into Ag. Incorporation of a small amount of Al suppresses the island formation of Ag film and facilitates continuous film growth. OPV devices based on Al-doped Ag films have enhanced performance compared to ITO ones due to advanced photon management. This study demonstrates that the Al-doped Ag film is a promising and effective alternative to current transparent conducting electrodes because of its simple deposition process, close-to-flatness, high transmittance, high conductivity, and easy device integration.

Supporting Information

Supporting Information is available from the Wiley Online Library or from the author.

Acknowledgements

This work was supported in part by the NSF Materials Research Science and Engineering Center (Program DMR 1120923) and ONR (N00014-12C0415) via a sub-contract through Soluxra Inc. We acknowledge the technical support of Lurie Nanofabrication Facility (LNF), especially Dr. Pilar Herrera-Fierro, Mr. Brian Armstrong, Mr. David Sebastian, and Dr. Vishva Ray. We appreciate support from Electron Microbeam Analysis Laboratory (EMAL), particularly Dr. Haiping Sun for the film characterization. D.Z. and C.Z. acknowledge Mr. Xin Xiao for assistance in EQE measurement and Dr. Yuan Li for useful discussion on simulation.

Received: December 12, 2013
Revised: May 17, 2014
Published online: June 18, 2014

[1] G. Subramania, A. J. Fischer, T. S. Luk, *Appl. Phys. Lett.* **2012**, *101*, 241107.
[2] R. Lazzari, J. Jupille, *Surf. Sci.* **2001**, *482*, 823.

[3] J. Gao, L. Sun, H. Deng, C. J. Mathai, S. Gangopadhyay, X. Yang, *Appl. Phys. Lett.* **2013**, *103*, 051111.
[4] L. Vj, N. P. Kobayashi, M. S. Islam, W. Wu, P. Chaturvedi, N. X. Fang, S. Y. Wang, R. S. Williams, *Nano Lett.* **2009**, *9*, 178.
[5] O. Inganas, *Nat. Photon.* **2011**, *5*, 201.
[6] D. S. Hecht, L. B. Hu, G. Irvin, *Adv. Mater.* **2011**, *23*, 1482.
[7] Y. Wang, S. W. Tong, X. F. Xu, B. Ozyilmaz, K. P. Loh, *Adv. Mater.* **2011**, *23*, 1514.
[8] D. Y. Liu, M. Y. Zhao, Y. Li, Z. Q. Bian, L. H. Zhang, Y. Y. Shang, X. Y. Xia, S. Zhang, D. Q. Yun, Z. W. Liu, A. Y. Cao, C. H. Huang, *ACS Nano* **2012**, *6*, 11027.
[9] D. Gupta, M. M. Wienk, R. A. J. Janssen, *Adv. Energy Mater.* **2013**, *3*, 782.
[10] M. G. Kang, H. J. Park, S. H. Ahn, L. J. Guo, *Sol. Energy Mater. Sol. Cells* **2010**, *94*, 1179.
[11] M. G. Kang, T. Xu, H. J. Park, X. G. Luo, L. J. Guo, *Adv. Mater.* **2010**, *22*, 4378.
[12] H. Wu, D. Kong, Z. Ruan, P.-C. Hsu, S. Wang, Z. Yu, T. J. Carney, L. Hu, S. Fan, Y. Cui, *Nat. Nano.* **2013**, *8*, 421.
[13] P.-C. Hsu, S. Wang, H. Wu, V. K. Narasimhan, D. Kong, H. Ryoung Lee, Y. Cui, *Nat. Commun.* **2013**, *4*, 2522.
[14] J.-Y. Lee, S. T. Connor, Y. Cui, P. Peumans, *Nano Lett.* **2008**, *8*, 689.
[15] F. S. F. Morgenstern, D. Kabra, S. Massip, T. J. K. Brenner, P. E. Lyons, J. N. Coleman, R. H. Friend, *Appl. Phys. Lett.* **2011**, *99*, 183307.
[16] M. G. Kang, L. J. Guo, *Adv. Mater.* **2007**, *19*, 1391.
[17] M. G. Kang, M. S. Kim, J. S. Kim, L. J. Guo, *Adv. Mater.* **2008**, *20*, 4408.
[18] M. G. Kang, H. J. Park, S. H. Ahn, T. Xu, L. J. Guo, *IEEE J. Sel. Top. Quantum Electron.* **2010**, *16*, 1807.
[19] J. G. Ok, M. K. Kwak, C. M. Huard, H. S. Youn, L. J. Guo, *Adv. Mater.* **2013**, *25*, 6554.
[20] A. Colsmann, A. Puetz, A. Bauer, J. Hanisch, E. Ahlswede, U. Lemmer, *Adv. Energy Mater.* **2011**, *1*, 599.
[21] D. W. Zhao, X. W. Sun, C. Y. Jiang, A. K. K. Kyaw, G. Q. Lo, D. L. Kwong, *Appl. Phys. Lett.* **2008**, *93*, 083305.
[22] X. W. Sun, D. W. Zhao, L. Ke, A. K. K. Kyaw, G. Q. Lo, D. L. Kwong, *Appl. Phys. Lett.* **2010**, *97*, 053303.
[23] R. S. Sennett, G. D. Scott, *J. Opt. Soc. Am.* **1950**, *40*, 203.
[24] M. Fahland, P. Karlsson, C. Charton, *Thin Solid Films* **2001**, *392*, 334.
[25] D. T. Nguyen, S. Vedraine, L. Cattin, P. Torchio, M. Morsli, F. Flory, J. C. Bernede, *J. Appl. Phys.* **2012**, *112*, 063505.
[26] J. N. Hilfiker, N. Singh, T. Tiwald, D. Convey, S. M. Smith, J. H. Baker, H. G. Tompkins, *Thin Solid Films* **2008**, *516*, 7979.
[27] M. Scalora, M. J. Bloemer, A. S. Pethel, J. P. Dowling, C. M. Bowden, A. S. Manka, *J. Appl. Phys.* **1998**, *83*, 2377.
[28] P. R. West, S. Ishii, G. V. Naik, N. K. Emani, V. M. Shalaev, A. Boltasseva, *Laser Photonics Rev.* **2010**, *4*, 795.
[29] J. F. Prins, *Mater. Sci. Eng. B* **1992**, *11*, 219.
[30] N. Wang, J. D. Zimmerman, X. Tong, X. Xiao, J. Yu, S. R. Forrest, *Appl. Phys. Lett.* **2012**, *101*, 133901.
[31] N. P. Sergeant, A. Hadipour, B. Niesen, D. Cheyns, P. Heremans, P. Peumans, B. P. Rand, *Adv. Mater.* **2012**, *24*, 728.
[32] B. O'Connor, C. Haughn, K.-H. An, K. P. Pipe, M. Shtein, *Appl. Phys. Lett.* **2008**, *93*, 223304.
[33] S. Auer, W. Wan, X. Huang, A. G. Ramirez, H. Cao, *Appl. Phys. Lett.* **2011**, *99*, 041116.
[34] C. C. Wu, C. I. Wu, J. C. Sturm, A. Kahn, *Appl. Phys. Lett.* **1997**, *70*, 1348.
[35] P. Yeh, *Optical Waves in Layered Media*, Wiley, New Jersey **1988**.